

Synthesis and Surface Behaviour of NDI Chromophores Mounted on a Tripodal Scaffold: Towards Self-Decoupled Chromophores for Single-Molecule Electroluminescence

Nico Balzer,^[a] Jan Lukášek,^[a] Michal Valášek,^{*,[a]} Vibhuti Rai,^[b] Qing Sun,^[b] Lukas Gerhard,^[b] Wulf Wulfhekel,^{*,[b, c]} and Marcel Mayor^{*,[a, d, e]}

Abstract: This paper reports the efficient synthesis, absorption and emission spectra, and the electrochemical properties of a series of 2,6-disubstituted naphthalene-1,4,5,8-tetracarboxdiimide (NDI) tripodal molecules with thioacetate anchors for their surface investigations. Our studies showed that, in particular, the pyrrolidinyl group with its strong electron-donating properties enhanced the fluorescence of such core-substituted NDI chromophores and caused a significant bathochromic shift in the absorption spectrum with a correspondingly narrowed bandgap of 1.94 eV. Cyclic voltammetry showed the redox properties of NDIs to be influenced by core substituents. The strong electron-donating character of pyrrolidine substituents results in rather high HOMO and

LUMO levels of -5.31 and -3.37 eV when compared with the parental unsubstituted NDI. UHV-STM measurements of a sub-monolayer of the rigid tripodal NDI chromophores spray deposited on Au(111) show that these molecules mainly tend to adsorb flat in a pairwise fashion on the surface and form unordered films. However, the STML experiments also revealed a few molecular clusters, which might consist of upright oriented molecules protruding from the molecular island and show electroluminescence photon spectra with high electroluminescence yields of up to 6×10^{-3} . These results demonstrate the promising potential of the NDI tripodal chromophores for the fabrication of molecular devices profiting from optical features of the molecular layer.

Introduction

With the growing demand of cheap and environmentally friendly electronic devices like organic light emitting diodes (OLEDs), the research field of molecular organic electronics gained increasing attention.^[1] Amongst others,^[2] various derivatives of naphthalene-1,4,5,8-tetracarboxdiimides (NDIs) are widely used for organic electronics due to their by core substituents tuneable electronic and optical properties,^[3] their chemical and photochemical stability,^[3,4] and their favourable electron transport properties.^[5,6] Consequently, OLEDs based on these subunits have been recently reported.^[7,8] Although Vollmann et al. first published this type of molecules already in the early 1930s,^[9] it was the group of Würthner who draw anew

the attention on NDIs and their core substituted derivatives.^[10] These NDI scaffolds with their large electron deficient aromatic system show reversible electrochemical reduction properties to form both, radical anions after one-electron reduction and dianions after two-electron reduction. Furthermore, physical and physicochemical properties of NDIs can be chemically optimised by substituents for particular purposes while the NDI core structure remains preserved. The electronic properties of NDIs can be adjusted by either electron withdrawing groups (EWGs) or/and electron donating groups (EDGs) at the core-positions and to a lesser extent at the axial positions of the NDI scaffolds. NDI scaffolds offer six positions for functionalisation divided mainly in two categories, namely the *N*-termini at the axial positions and the naphthalene core. Functionalisation of


[a] N. Balzer, J. Lukášek, Dr. M. Valášek, Prof. Dr. M. Mayor
Institute of Nanotechnology
Karlsruhe Institute of Technology
P.O. Box 3640, 76021 Karlsruhe (Germany)
E-mail: michal.valasek@kit.edu


[b] V. Rai, Q. Sun, Dr. L. Gerhard, Prof. Dr. W. Wulfhekel
Institute of Quantum Materials and Technologies
Karlsruhe Institute of Technology
76021 Karlsruhe (Germany)
E-mail: wulf.wulfhekel@kit.edu

[c] Prof. Dr. W. Wulfhekel
Physikalisches Institut, Karlsruhe Institute of Technology
Wolfgang-Gaede-Straße 1, 76131 Karlsruhe (Germany)

[d] Prof. Dr. M. Mayor
Department of Chemistry, University of Basel
St. Johannis-Ring 19, 4056 Basel (Switzerland)
E-mail: marcel.mayor@unibas.ch

[e] Prof. Dr. M. Mayor
Lehn Institute of Functional Materials
School of Chemistry, Sun Yat-Sen University
Guangzhou, Guangdong 510275 (P. R. China)

 Supporting information for this article is available on the WWW under <https://doi.org/10.1002/chem.202101264>

 © 2021 The Authors. Chemistry - A European Journal published by Wiley-VCH GmbH. This is an open access article under the terms of the Creative Commons Attribution Non-Commercial NoDerivs License, which permits use and distribution in any medium, provided the original work is properly cited, the use is non-commercial and no modifications or adaptations are made.

the axial *N*-imide positions of NDI mainly influences its solubility^[11] or morphology in thin films,^[12] while having negligible effect on the optoelectronic properties. On the other hand, the chemical substitution at the 2, 3, 6 and 7 positions of the NDI core with various groups, such as alkyl or arylamino, alkoxy, sulfanyl, cyano, thiophene and different heterocycles, considerably tune their electronic and photophysical properties. Therefore, molecular engineers use these positions to fine-tune the HOMO and LUMO energy levels of the NDI core in order to obtain model compounds with tailor-made optical and electronic properties.^[3,10,13] The ability to change both, colour and redox properties without global structural changes is the most attractive characteristics of core-substituted NDIs. Since the 2000s, many groups have developed various strategies to core substitute NDIs with electron donating heteroatoms like S, O or N and thus create push-pull systems with the electron poor NDI core to modulate the absorption and emission properties of the organic chromophore.^[10,13,14] The colours of core-substituted NDIs originate from a charge transfer band that moves to the red over the full rainbow spectrum with increasing push-pull character between the core substituent and the NDI core. While photoluminescence properties of NDIs have been extensively studied,^[3] their electroluminescence behaviour is barely studied.^[7,8] Given their synthetic accessibility, tuneable photophysical properties, reversible electrochemistry,^[15,16] ground- and excited state stability, and structural integrity, NDIs are particular appealing chromophores for the development of model compounds to investigate single molecule electroluminescence. However, to the best of our knowledge, only few studies have been published so far.^[17,18]

Fathoming the underlying light emission processes from these molecules is thus not only interesting from a scientific point of view, but also key for the development of new materials for optoelectronic devices. Scanning tunnelling microscopy induced luminescence (STML) experiments enable to study electrically induced light emission and the underlying mechanisms of the optoelectronic response with submolecular precision.^[19–21] Using STML setups, various pathways for single molecule light emission have been discovered at the single molecule level, including dipole–dipole coupling, hot electroluminescence, plasmon-exciton coupling, and electrofluorochromism.^[22–25] However, in order to observe electroluminescence from single organic chromophores in STML experiments, the chromophore must be electronically decoupled from the underlying metal substrate to compete with quenching of the molecule's excited state by the metal's electrons.^[26,27] Common approaches to achieve such isolation of individual chromophores are either ultrathin (in)organic insulating layers with large band gaps of several electron volts between the metal surface and chromophores,^[26–29] or multilayered stacks of the chromophore.^[30] Alternative, less explored strategies to electronically decouple organic emitters from the underlying surface involve either bulky spacer groups within the tailor-made molecule or large multipodal platforms.^[31,32] The latter has been recently applied for example with a fully symmetric tetrapodal molecule, from which three functional arms served as tripod and the fourth arm was perpendicularly

arranged in an upward direction,^[33] or by separating the chromophore subunit with a rigid multipodal anchoring scaffold.^[34–36] The modular strategy of electronically decoupling via a rigid multipodal platform not only enables the investigation of a variety of chromophores, but also allows to align the chromophore's dynamic dipole vector perpendicular to the surface resulting in enhanced luminescence.^[37]

Here we report the design, synthesis and characterisation of the three molecules **Tpd-hNDI**, **Tpd-sNDI** and **Tpd-nNDI** (with *h/s/n* representing the (hetero)atom directly connected to the NDI core) as molecular emitters mounted on a tripodal scaffold as displayed in Figure 1a), together with first STM and STML studies of their (sub)monolayers obtained by spray deposition and subsequent annealing on Au(111) surfaces. While the molecular design is geared towards upright standing NDI chromophores fixed by the tripodal platform (Figure 1b), we learned in the past with model compounds comprising tetraphenylmethane based tripodal platforms about their hardly predictable surface behaviour.^[38,39] Thus the scanning probe experiments enable to shed light on whether the three potential covalent sulfur gold bond of the tripodal platform dominate the monolayer formation and provide upright standing chromophores as displayed in Figure 1b), or the van der Waals attraction between the surface and the chromophore's extended π -system dominate the molecule's surface behaviour as sketched in Figure 1c). In addition to the parent NDI structure, amino and sulfanyl groups are considered as core substituents to cover a broad range of emission wavelengths. Phenylacetylene serves as a linker to maintain the molecular rigidity and efficiently decouple the NDI emitter from the tripodal platform. The tripodal design of the foot structure with three thiol anchoring groups in the *meta*-positions was chosen with the intention to provide a rigid, covalently bonded anchor to the Au(111) surface with an upright orientation of the protruding functionality.^[40] These tripodal molecules with acetyl protected anchoring groups can be efficiently deprotected either *in situ*^[40,41] upon binding to the gold surface or chemically by cleaving agents.^[42] With this strategy, we aim to enable self-decoupling of NDI chromophores from the substrate by molecular design. The scope of the present study is not only the synthesis of the target molecules **Tpd-hNDI**, **Tpd-sNDI** and **Tpd-nNDI**, but also to study their photophysical and electrochemical properties and surface investigations with the STML setup.

It should be noted that the stabilisation of the functional tripodal molecules on metallic surfaces is a subtle balance which is attributed both to the lateral van der Waals interactions for example between flat delocalised π -systems and to the chelate effect of the tripodal scaffolds. Therefore, one has to consider the competing binding energies of the two potential anchoring sites of functionalised tripods, namely the functional unit-surface interface and the degree of chelation via thiolate anchors of the molecular tripod in a commensurate order to the gold surface. If the interactions between functional unit and surface is larger than the energy gained by the foot structure, the molecules will adsorb flat on the surface.^[38] Thus, the proposed tripodal platforms exposing large NDI chromo-

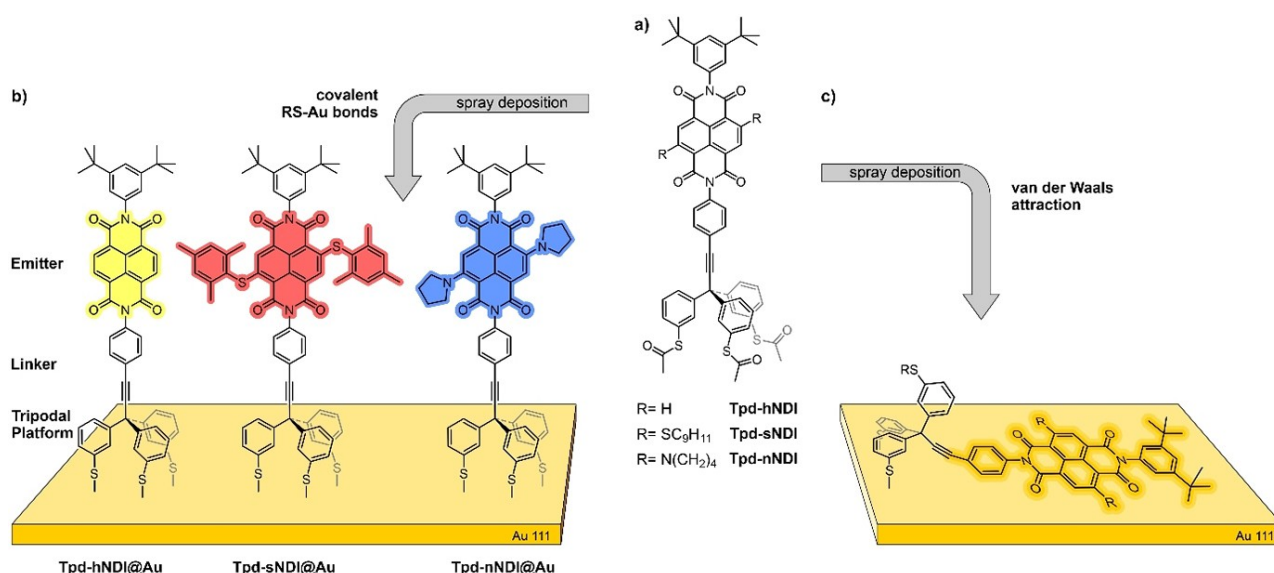


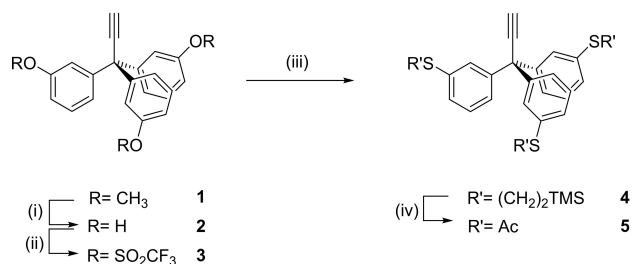
Figure 1. a) Series of the tripodal platforms with NDI chromophores **Tpd-hNDI**, **Tpd-sNDI** and **Tpd-nNDI** and b) their intended arrangement on a Au(111) substrate, with the colour code of NDI emitters representing their solution colours. c) Expected arrangement of the model compounds on the substrate in case of dominating van der Waals attractions.

phores are good candidates to investigate how such extended molecules arrange on the substrate.

Results and Discussion

Design and synthesis of molecules

The synthetic approach towards a rigid tripodal platform **4** is based on a triphenylmethane derivative and displayed in Scheme 1.^[34,40,43] Introducing a triple bond on the sp^3 -hybridised carbon atom of the tripodal platform is expected to provide the compactness required for STM based investigations and enables to modularly develop the structure through Sonogashira coupling chemistry. Note, that a comparable foot structure based on a tetraphenylmethane scaffold has been recently used in single molecule light emission experiments by Hou et al., but significant differences are expected in the sturdiness of the tripod-Au(111)-interface arrangement due to the used benzylth-

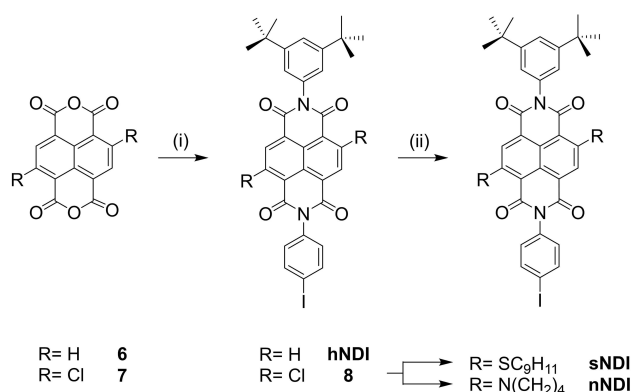


Scheme 1. Synthesis of the tripodal platforms. i) sodium ethanethiolate, DMF, 83 %; ii) Tf_2O , Et_3N , 73 %; iii) 2-(trimethylsilyl)ethanethiol, Xantphos, $Pd_2(dba)_3$, 80 %; iv) $AgBF_4$, $AcCl$, 92 %.

iol anchor groups.^[34] In the here presented tripod design, the aromatic thiol anchors allow direct connections to the gold substrate avoiding additional flexibility due to CH_2 linkers. The intention is to improve both, the electron transport and the rigidity of the spatial arrangement, hopefully controlling an upright orientation of the molecular rods on the gold substrate.

The synthesis of 3,3,3-tris(3-methoxyphenyl)propyne **1** was previously reported by Garcia-Garibay et al.^[44] While the demethylation of **1** with commonly used Lewis acids such as BBr_3 would require an additional protection of the triple bond to avoid its borylation,^[45] a method originally published by Feutrill and Mirrington involving sodium ethanethiolate in DMF as demethylation agent was used to afford the desired product **2** in 83 % yield.^[46] The following step was triflation of triol **2** with triflic anhydride to yield triflate **3** in 73 %. In the next step, the thiol anchor groups were introduced in their TMS-ethyl-protected form. The triflate **3** was converted by the C–S cross-coupling reaction with 2-(trimethylsilyl)ethanethiol in the presence of palladium catalyst and Xantphos ligand to the desired product **4** with a yield of 80 %. Subsequent trans-protection of the thiols in **4** was performed using $AgBF_4$ and acetyl chloride in dichloromethane to afford the desired thioacetate **5** in very good yield of 92%.^[47] Unfortunately, the thioacetate groups did not provide the stability required for the Sonogashira coupling reactions disqualifying the modular plan of decorating the platform in the last step with the NDI chromophores. As second best alternative the 2-(trimethylsilyl) ethyl protected derivative **4** was used for the assembly between NDI chromophore and platform, followed by a final trans-protection step to get the target molecules as thioacetates.

NDI derivatives **hNDI**, **sNDI** and **nNDI** suitable for their assembly with the tripodal platform were synthesised as shown in Scheme 2. 2,6-Dichloronaphthalene-1,4,5,8-tetracarboxylic



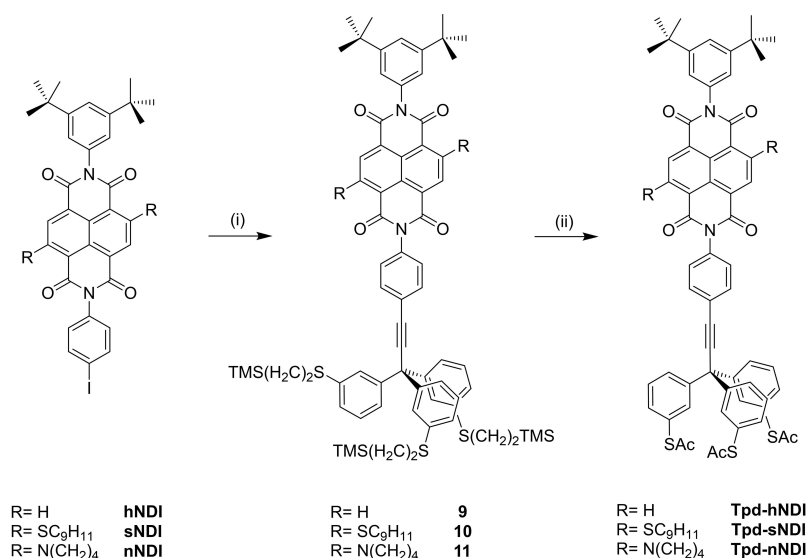
Scheme 2. Synthesis of NDI chromophores. i) 3,5-di-*tert*-butylaniline, *p*-iodoaniline, AcOH, 43% (39% for compound **8**); ii) for **sNDI**: 2,4,6-trimethylthiophenol, K₂CO₃, 69%; for **nNDI**: pyrrolidine, K₂CO₃, 99%.

acid dianhydride **7** was synthesised in four reaction steps by following a literature procedure.^[9] The twofold amide condensation with two different aniline derivatives to obtain asymmetric naphthalene-1,4,5,8-tetracarboxydiimides turned out to be more challenging than expected. In the case of unsubstituted **hNDI**, the classical step-by-step approach was followed to obtain **hNDI** with an overall yield of 43%. Unfortunately, in the case of 2,6-dichlorinated NDI **8**, this approach was not successful because such disubstituted-core derivatives are more soluble in organic solvents and prone to nucleophilic substitutions at the 2 and 6 positions, resulting in considerable material loss due to a number of core-substituted NDIs as side products. As alternative a one-pot reaction with an equimolar stoichiometric ratio of both anilines was performed, expecting a statistical distribution of all possible products. To our delight, the desired NDI derivative **8** was isolated as a yellow powder in 39% yield with an optimised procedure. In particular, the reaction temperature was decreased to room temperature from initially 100 °C and the anilines were deactivated by stirring for 30 minutes in acetic acid prior their addition to the dianhydride **7**. For the amide condensation, aniline derivatives were chosen carefully so that one has the iodine moiety attached in the *para* position to further interlink the NDI chromophore with the tripodal platform **4** through a Sonogashira protocol, while the second one bears two *tert*-butyl groups in the *meta* positions providing both, the solubility required for further processing and the compactness favouring STM experiments. Although NDI solubility could have also been increased by using (long and branched) alkyl chains, their flexibility and bulkiness could handicap the arrangement of the target molecules upright on the metallic surface. Although benzylic core substituted NDIs are known to be more fluorescent than their phenyl counterparts,^[48] 2,4,6-trimethylthiophenol and pyrrolidine were selected as substituents while benzylic substituents might be more prone to degradation in the final transprotection step. Core-functionalisation of **8** with 2,4,6-trimethylthiophenol in a nucleophilic aromatic substitution reaction gave a red **sNDI** in 69% yield. Methyl groups in the *ortho* positions of 2,4,6-trimethylphenyl substituent are increasing its steric hindrance

and thus prevent their further substitution under harsh conditions in the final transprotection step. Initially carbazoles were considered as amino substituents, however their reactivity in S_NAr reaction with **8** was too low and did not lead to the desired product. Moreover, primary alkyl amines as NDI core substituents were avoided, because particular decay mechanisms were suggested for substituents containing an α -proton next to the heteroatom. In particular their fluorescence might be quenched either by electron transfer into the SOMO (former HOMO) of the chromophore, or by the formation of intramolecular hydrogen bonds between the α -proton and the closed carbonyl group, resulting in a radiation less decay of the excited state.^[10,48] Therefore, pyrrolidine was used for the substitution of **8** in the 2 and 6 positions to obtain **nNDI** in almost quantitative yield as a blue solid. As already indicated by the colour change of all three NDIs, the electron donating character of substituents is also observed in ¹H NMR spectra which is associated with a general upfield shift of the NDI-core protons with an increasing number of electron donating groups.

Comparing the chemical environment of the NDI-core protons, core-substitution with 2,4,6-trimethylthiophenol results in a chemical shift of 8.04 ppm and 8.01 ppm for the NDI core protons, while substitution with pyrrolidine leads to a chemical shift of the core protons to 8.43 ppm and 8.40 (for NMR spectra see Figures S22 (**sNDI**) and S28 (**nNDI**) in the Supporting Information). The unsubstituted **hNDI** core protons show the most deshielded chemical shift of 8.84 ppm (Figure S14).

The final assembly of the target molecules **Tpd-hNDI**, **Tpd-sNDI** and **Tpd-nNDI** is outlined in Scheme 3. After successful isolation of all NDIs, Sonogashira reaction was used to couple **hNDI**, **sNDI** and **nNDI** respectively with the modular platform **4** to afford precursors **9–11** in 67, 46 and 78% yield, respectively. THF was used as co-solvent for the Sonogashira cross-coupling reaction because of poor solubility of the NDI-precursors in neat amines (Et₃N, etc.). Final transprotection of the thiols in **9–11** was successfully performed using AgBF₄ and acetyl chloride in dichloromethane to afford the desired thioacetate masked target structures **Tpd-hNDI**, **Tpd-sNDI** and **Tpd-nNDI** in good yields. Note, that the acetyl protected target molecules in solution at ambient conditions are only moderately stable. Therefore, solvent evaporation must be carried out at room temperature, otherwise thiol deprotection and subsequent polymerisation to for example disulfides was observed. Also, long retention times on column chromatography leads to a significant decrease in isolated yield. The introduction of the tripodal structure had no impact on the electronic structure of the NDI chromophore, as very comparable photophysical properties and chemical shifts of the NDI cores were observed for precursors and target structures (see Figures S1, S14, S16 and S18 for **hNDI**, **9**, **Tpd-hNDI**; Figures S2, S22, S24 and S26 for **sNDI**, **10**, **Tpd-sNDI**; Figures S3, S28, S30 and S32 for **nNDI**, **11**, **Tpd-nNDI**).^[49] All target molecules were purified by chromatography and fully characterised by conventional analytical and spectroscopy techniques like NMR spectroscopy, mass spectrometry, IR, UV-Vis and fluorescence spectrometry, as well as by elemental analysis. More details on the synthesis and purifica-



Scheme 3. Synthesis of the target tripodal molecules. i) 4, CuI, Pd(PPh₃)₄, Et₃N, THF, 67% (**9**), 46% (**10**) and 78% (**11**); ii) AcCl, AgBF₄, CH₂Cl₂, 93% (**Tpd-hNDI**), 82% (**Tpd-sNDI**), 69% (**Tpd-nNDI**).

tion of all new compounds and their characterisation are provided in the Experimental Section and in the Supporting Information.

Spectrophotometric studies

UV/Vis absorption and fluorescence spectra were recorded in dichloromethane with a concentration of about 25 μM and are shown in Figure 2 and summarised in Table 1. The absorption and emission properties of **Tpd-hNDI**, **Tpd-sNDI** and **Tpd-nNDI** noticeably depend on the core substitution. Absorption bands can be divided into three different parts. The central absorption bands at around 350 nm, which show the π–π* transition and their vibrational fine structure of the three different chromophores, barely differ upon substitution, which is in accordance with the literature.^[10] Moreover, the peaks in the UV region (~300 nm) do not significantly change upon core-substitution, whereas they are missing in unsubstituted **Tpd-hNDI**.^[13] The rise of a new charge-transfer band in the visible region, which is introduced by and strongly depending on the push-pull character of the core substitution is associated with the colours. Whereas unsubstituted **Tpd-hNDI** is pale yellow in CH₂Cl₂ solution, **Tpd-sNDI** is red (λ_{max} = 524 nm) and **Tpd-nNDI** is blue (λ_{max} = 602 nm). The remarkable bathochromic shift in the absorption maxima of the amino substituted NDI **Tpd-nNDI** can be related to the stronger electron donating effect (+M effect) of the pyrrolidine substituent on the frontier molecular orbitals of the NDI core.^[48] In case of **Tpd-nNDI**, this intramolecular charge transfer can be hindered by mono protonation with HCl or even switched off by total protonation and reversibly restored.^[50] The absorption maxima at 524 nm with a shoulder at 492 nm (**Tpd-sNDI**) and at 602 nm with a shoulder at 558 nm (**Tpd-nNDI**) are quite broad.^[50] In contrast to previous reports, our 2,4,6-trimethylphenylsulfanyl core-substituted NDI chromophore shows fluorescence at 557 nm with a broad emission band,^[17,48] however the quantum yield is low and cannot be reproducibly measured. For pyrrolidine core-substituted **Tpd-nNDI** the emission maximum is observed at 627 nm. The Stoke

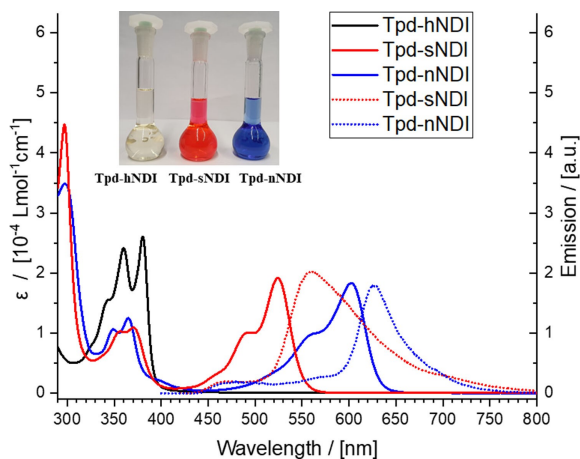


Figure 2. UV/Vis absorption spectra (solid line) of **Tpd-hNDI** (black), **Tpd-sNDI** (red), **Tpd-nNDI** (blue) and normalised emission spectra (dotted line). Recorded in CH₂Cl₂ with a concentration of 25 μM at ambient temperature. A photograph of **Tpd-hNDI** (left), **Tpd-sNDI** (middle) and **Tpd-nNDI** (right) solutions in CH₂Cl₂ is shown in the inset.

Molecule	λ _{abs} [nm] (ε [Lmol ⁻¹ cm ⁻¹])	λ _{em} [nm]
Tpd-hNDI	360 (24995), 381 (26976)	n.d.
Tpd-sNDI	297 (50638), 357 (10053), 370 (10620), 524 (19231)	557
Tpd-nNDI	298 (32790), 349 (9600), 365 (11463), 602 (17376)	627

shift, that is the difference between the absorption and emission maxima, is 33 nm for the **Tpd-sNDI** chromophore and 25 nm for **Tpd-nNDI** chromophore.^[3] The emission intensity and the fluorescence quantum yield significantly decreases from **Tpd-nNDI** to **Tpd-sNDI** and no fluorescence has been observed for unsubstituted **Tpd-hNDI** derivative.

Electrochemical properties

Cyclic voltammetry (CV) in CH_2Cl_2 against ferrocene/ferrocenium (Fc/Fc^+) was conducted to further investigate the influence of core substitution upon the electrochemical properties of all chromophores **hNDI**, **sNDI** and **nNDI** (Figures 3 and S4, Table 2). The half-wave potential values $E_{1/2}$ were calculated as the arithmetical mean of the anodic and the cathodic peak potentials. To calculate the LUMO energy levels (against vacuum), the onset reduction potentials $E_{\text{onset}}^{\text{red1}}$ versus the Ag/Ag^+ reference electrode of each NDI were taken and subtracted from the Fc/Fc^+ standard (using -4.8 eV). It is assumed that the redox potential of Fc/Fc^+ has an absolute energy level of 4.8 eV to vacuum.^[51] The HOMO energy is determined from the LUMO level minus the HOMO/LUMO gap, which is available from absorption spectra at the long wavelength absorption edge ($E_{\text{gap}}^{\text{opt}} = 1240/\lambda_{\text{onset}}$).^[52] Such determination of optical as well as

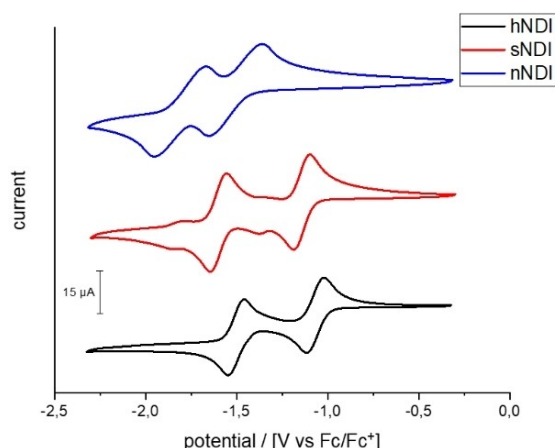


Figure 3. Cyclic voltammograms in the cathodic region of **hNDI** (black), **sNDI** (red) and **nNDI** (blue) recorded in CH_2Cl_2 containing a 0.1 M solution of Bu_4NPF_6 as a supporting electrolyte. Fc/Fc^+ was used as an internal reference. Scan rate: 100 mVs^{-1} .

Chromophore	$E_{1/2}^{\text{red1}}$	$E_{1/2}^{\text{red2}}$	E_{LUMO}	$E_{\text{gap}}^{\text{opt}}$	E_{HOMO}
hNDI	-1.10 V	-1.53 V	-3.80 eV	3.17 eV	-6.97 eV
sNDI	-1.14 V	-1.62 V	-3.72 eV	2.24 eV	-5.96 eV
nNDI	-1.43 V	-1.77 V	-3.37 eV	1.94 eV	-5.31 eV

electrochemical band gap from peak values is mainly based on the detailed quantum chemical calculations of Brédas et al. who found a linear correlation between ionisation potential and oxidation potential and also between electron affinity and reduction potentials.^[53] Note, that small differences between optical HOMO/LUMO gap and the electrochemical gap are expected not only because of the intrinsic experimental uncertainties but also because charged molecules are compared to neutral ones.^[54]

All three NDIs show two reversible reduction processes, implying the formation of radical anions and dianions, which are separated by 0.34, 0.43 and 0.48 V for **nNDI**, **hNDI** and **sNDI** respectively. In case of **nNDI**, the electron donating core substitution, namely pyrrolidine, results in destabilising the radical anion and shifting the reduction to the more negative potentials. A gradual shift of the reduction potentials to more negative values for the core substituted NDIs reveals a direct relationship between the electron-donating properties of the core substituents and the electrochemical properties of NDIs. Additional irreversible oxidation waves were observed for **nNDI** at around $+0.6$ and $+0.8$ V against Fc/Fc^+ (Figure S4). To prevent irreversible oxidations, the CV was carried out only in the cathodic region. Thus, both **hNDI** and **sNDI** chromophores were also measured between -2 and 0 V. The amino substituted **nNDI** chromophore showed reduction potentials at -1.43 and -1.77 V that are in the same range as previously observed for the similar amino core-substituted NDIs.^[49,50,55] The LUMO energy estimated from the CV is -3.37 eV resulting in the HOMO energy level of -5.31 eV, which is comparable to previously reported results.^[50] However, each of the two anodic and cathodic peak potential pairs differ for about 0.3 V. Electrode films of some newly formed species as an explanation for these broad peaks can be excluded, since the experiments were carried out with freshly cleaned electrodes and are reproducible over several measurements. As seen from the cyclic voltammograms in Figure 3, the sulfanyl core substitution in **sNDI** decreases the electron donating character compared to the amino derivative **nNDI**. Hence the reduction potential values (-1.14 and -1.62 V) of **sNDI** are shifted towards more positive potentials, corresponding to a LUMO energy level of -3.72 eV and a HOMO energy level of -5.96 eV. The obtained values are comparable with previously published results on alkylsulfanyl and arylsulfanyl core-substituted NDIs.^[56,57] Within this series, the core-unsubstituted compound **hNDI** exhibits the most positive reduction potentials of -1.10 and -1.53 V. Comparing the **sNDI** and **hNDI** chromophores, the donating character of the arylsulfanyl group is clearly observed in the second reduction $\text{NDI}^{\bullet-}/\text{NDI}^{2-}$ but significantly less in the first reduction $\text{NDI}/\text{NDI}^{\bullet-}$. This suggests that arylsulfanyl as a core substituent destabilises the dianion more than the radical anion. The LUMO energy level of **hNDI** is calculated to be -3.80 eV, which results in the HOMO energy of -6.97 eV. The HOMO–LUMO optical gaps were calculated from the onset of the lowest energy absorptions to approximate the HOMO energies and the obtained values are listed in Table 2.

Scanning tunnelling microscopy induced luminescence experiments

The surface behaviour of all three tripodal molecules bearing NDI chromophores was investigated using STML at 5 K in UHV. Spray deposition of about 1 μL of **Tpd-hNDI** solution ($c \sim 1 \text{ mg/mL}$, for details see the Experimental Section) with a post annealing temperature of 100 °C leads to the formation of unordered islands of about 0.3 nm in height (Figure 4a). This height indicates that the molecules are not adsorbed as intended but rather adsorb flat on the metal surface. While the islands seem to be composed of identical objects with clear substructure, the lack of any long-range order makes an assignment of the molecular adsorption impossible. When the STM tip is placed above these islands, plasmonic light emission which is characteristic for noble metal nanogaps,^[21] is partially or fully suppressed and the molecular layer merely acts as a dielectric layer that lowers the emission intensity.^[58] At some positions, molecular clusters of more than 1 nm in height protrude from the molecular islands (Figure 4b). STM images of these clusters typically show white streaks and abrupt changes in the apparent height from one horizontal scan line to the next. These are signs of instability of the tunnel junction and can be explained by multilayers of **Tpd-hNDI** molecules of unknown orientation or by standing molecules in a less stable configuration as compared to the ordered monolayer. On these clusters and in the close vicinity, some light emission spectra are clearly different from a plasmonic light emission. We recorded 2500 photon spectra at different positions across the two clusters as depicted in Figure 4b. At most positions, the photon spectra are similar to the grey spectrum shown in Figure 4c recorded at the position indicated by the grey cross in Figure 4b, with a broad peak centred around 1.5 eV. While the precise energy of the plasmonic resonance might shift depending on the exact position and the shape of the tip apex,^[19,59] the FWHM of about 300 meV indicates a plasmonic origin. About 200 out of 2500 spectra recorded on this area have a clearly different appearance and exhibit one or more sharper peaks of 30 to 100 meV FWHM to which we therefore tentatively assign a molecular origin. Six examples of such photon spectra are shown in Figure 4c (coloured photon spectra). The peak position ranges from 1.5 to 2.05 eV within the measurement on the area shown in Figure 4b. The quantum yield, that is the number of photons emitted per tunnelling electron, ranges from 1×10^{-4} to 1×10^{-3} for an applied sample bias of -2.5 V . Neither the spectral shape nor the quantum yield can be definitely related to the position where the spectrum has been recorded (that is the topography) and small displacements of the STM tip may lead to drastic variations of the photon spectrum (compare, e.g., the grey and dark blue spectra in Figure 4c). This can be explained by the large number of possible adsorption configurations and the absence of long-range order which lead to a number of different electronic environments for each molecule. The orientation with respect to the substrate, the orientation with respect to the electric field present in the STM junction and the coupling to neighbouring molecules varies for each molecule under inves-

tigation. In addition, there might be different charge states of the molecule involved which drastically influence the emission energy.^[25,37] Still, at fixed positions, the junction is stable enough to perform extended measurements.

This allows to record photon spectra as a function of the applied sample bias which defines the energy of the tunnelling electrons. Figure 4d shows such spectra recorded at the position marked by the red cross in Figure 4b. In this experiment, light emission sets in for a sample bias above +1.8 V and below -2 V with photon energies of less than 1.7 eV, reflecting the asymmetry of the STM junction under reversion of the polarity of the applied voltage.^[22,63] For low currents and low temperatures, the high energy edge of a photon spectrum of plasmonic origin is expected to be limited by the energy provided by the tunnelling electrons: $eV = h\nu$. However, the threshold values for light emission observed in Figure 4d are clearly higher than the high energy edge of the photon spectra, which is a clear sign of molecular contribution to the light emission. In addition, both peaks emerge at the same bias voltage, which indicates that the redshifted peak can be attributed to the same molecular transition with an additional excitation of a molecular vibration,^[26,60] $eV = h\nu + \hbar\omega$. Indeed, most photon spectra recorded on the unordered clusters of **Tpd-hNDI** show a series of peaks with a typical spacing of about 160 meV (see also Figure S34c), in full agreement with a recent study on tetrapodal perylene diimides (PDIs) on Au(111).^[33] Rarely, light emission above the quantum threshold has been observed, even at low currents, which is an indication for intramolecular up-conversion (Figure S34b).^[61]

The combination of our highly efficient photon collection setup^[20] and an efficient conversion process in the molecular junction results in unusually high count rates observed for **Tpd-hNDI**. The spectrum recorded at 2.5 V and 5.2 pA shown in Figure 4d corresponds to 1.3×10^{-3} photons counted per tunnelling electron, which is, to best of our knowledge, about one order of magnitude higher than the highest external quantum yields reported so far.^[19,62] After correction by the detector efficiency, this results in an internal quantum yield of about 6×10^{-3} .

After annealing, the **Tpd-hNDI** sample for a second time, at 180 °C, ordered island structures form. Figure 5a shows a typical island which exhibits a monoclinic lattice structure with a unit cell (red lines) of $2.7 \text{ nm} \times 4.04 \text{ nm}$ ($\alpha = 53^\circ$) = 8.6 nm^2 . The apparent height of about 0.3 nm of these islands (see cross section along the white line in Figure 5a) is similar to that of the unordered ones discussed above and indicates that the **Tpd-hNDI** molecules adsorb in a horizontal configuration. In comparison, at similar voltages, a naphthalene diimide cyclophane “double decker” has been reported to show an apparent height of about 0.7 nm.^[18] Although the precise adsorption configuration is difficult to infer from the topographic image, we suggest a pairwise alignment as outlined in Figure 5b so that each bright blob corresponds to one molecule. This would result in an area of 4.3 nm^2 covered per molecule.

Similar to the unordered flat islands, plasmonic light emission is strongly suppressed when the tip is placed on top of the ordered islands. Figure 5c shows examples of photon

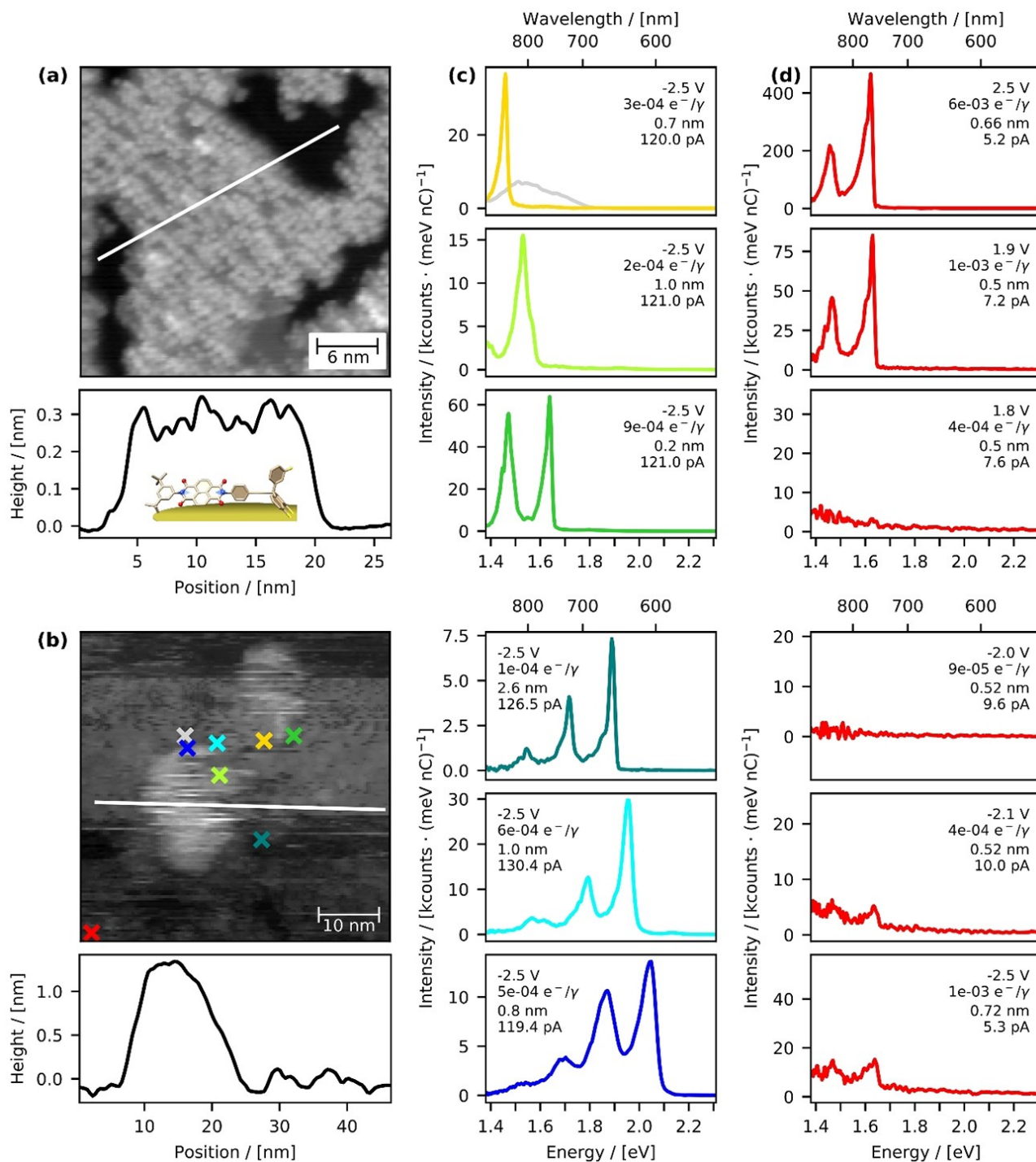


Figure 4. Light emission from unordered clusters of **Tpd-hNDI**. a) Typical island structure of **Tpd-hNDI** with clean (black) areas of Au(111) in between. The cross section taken along the white line reveals an apparent height of the island of about 0.3 nm. The molecular model in the proposed orientation is not to scale. Sample bias: 1.8 V, tunnelling current: 5 pA. The scan frame is 30 nm wide. b) Two clusters of **Tpd-hNDI** (bright areas) with an apparent height of 1.2 nm (see cross section along the white line) above the island (darker areas). Sample bias: -2.3 V, tunnelling current: 5 pA. The scan frame is 50 nm wide. c), d) Photon spectra recorded at the positions indicated by the corresponding crosses in (b). The applied sample bias, the internal quantum yield (count rate corrected for detector efficiency), the vertical z-position of the tip and average current during the acquisition are indicated in each panel. Integration time is 2 s. Bias voltage, yield and average current during the acquisition as indicated in the graphs c), d).

spectra with the tip placed above Au(111) (red curve) and placed above the molecular island (black curve). While there are expected small intensity variations superimposed to a broad

plasmonic spectrum in both curves, sharp peaks of molecular origin as described in Figure 4c are absent.

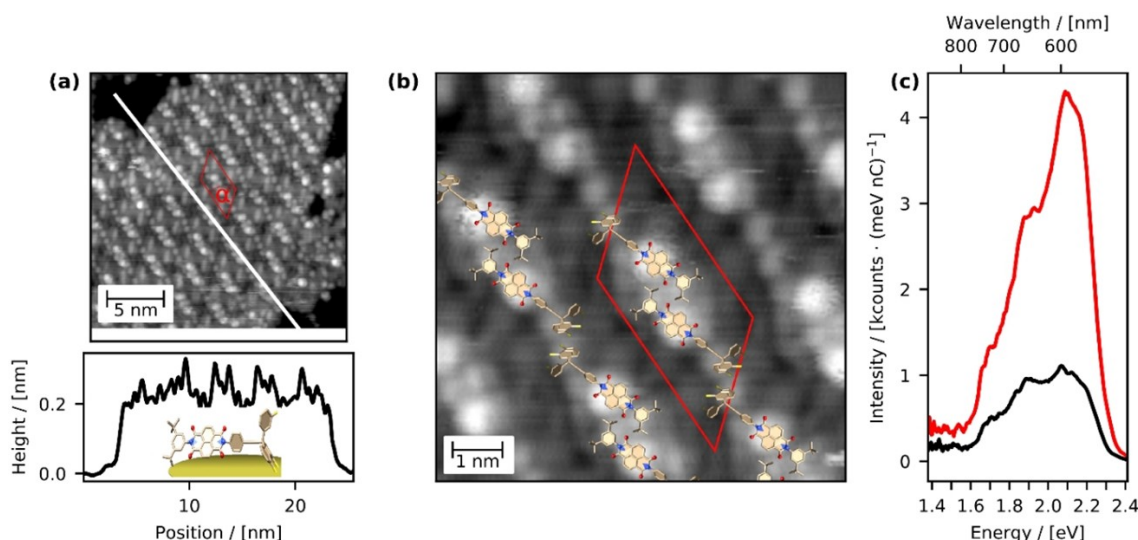


Figure 5. Ordered structure of **Tpd-hNDI**. a) Ordered island of **Tpd-hNDI** with a unit cell indicated in red. Black areas correspond to empty Au(111) surface. The cross section taken along the white line shows an apparent height of about 0.3 nm. Molecular model not to scale. Sample bias: 2.1 V, tunnelling current: 9 pA, scan width: 22 nm. b) Close-up scan of an ordered island with the unit cell indicated in red and molecular models of **Tpd-hNDI** superimposed to scale in the suggested adsorption configuration. Sample bias: -2.1 V, tunnelling current: 5 pA, scan width: 8 nm. c) Typical photon spectra recorded on the ordered islands (black) and the nearby Au(111) surface (red). Sample bias: 3 V, tunnelling current: 140 pA, integration time: 2 s.

Similar to **Tpd-hNDI**, the core-substituted variant **Tpd-sNDI** forms unordered islands of about 0.3 nm in apparent height as is shown in Figure 6a at a post annealing temperature of 100 °C. In addition, these islands act as a dielectric that reduces light emission from the decay of local gap plasmons, similar to Figure 5c. While we cannot exclude formation of clusters at 100 °C, we only observed such clusters of increased height after annealing a second time, to 180 °C. Figure 6b shows an example of a cluster that exceeds the surrounding island by 0.2 to 0.4 nm in apparent height. With the STM tip placed above these clusters, we observe light emission with two pronounced peaks that are typically separated by about 160 to 170 meV. We have seen the same spacing for the spectra of **Tpd-hNDI** (Figures 4c and S34c) which corresponds to the energy of the C–N stretch mode. Therefore, we assume that also in the case of **Tpd-sNDI** the red shifted peak originates from a decay from the first electronically excited state to the vibrationally excited electronic ground state. Apparently, the local surrounding has a significant influence on both the electroluminescence efficiency and the energy of the emitted light. In agreement with the recent study on PDI tripodal molecules,^[33] the molecular configuration seems to be easily influenced by the nearby tip which hampers reproducibility of STML experiments. The wavelength shift of the substituted NDI molecules compared to the unsubstituted chromophore as it is observed in our PL measurements, does not translate to a shift of the electroluminescence photon spectra of the molecules deposited on the Au(111) surface.

Similar to **Tpd-hNDI**, **Tpd-sNDI** forms well-ordered islands at elevated post-annealing temperatures of 180 °C (Figure 6d). The apparent height of 0.3 nm suggests that these islands are composed of flat-lying molecules, which is in agreement with the absence of any molecular signature in the photon spectra on these islands. A close-up scan of an ordered island shown in

Figure 6d reveals a rich sub-molecular structure. We propose an adsorption configuration similar to the case of **Tpd-hNDI** (Figure 5b): Molecular pairs arrange in chains with the foot group pointing towards the next pair (Figure 6e). Molecules of adjacent chains are mirrored. A closer look at the edges of the molecular island shows one quarter of the unit cell as the smallest unit, which confirms the hypothesis of pairwise adsorption (Figure S34d). In this rather tightly packed configuration, the unit cell with an area of $3.3 \text{ nm} \times 5.0 \text{ nm}$ ($\alpha = 47.6^\circ$) = 12.2 nm^2 contains 4 molecules (= 3.05 nm^2 per molecule).

The third NDI tripod, **Tpd-nNDI**, also forms unordered islands of about 0.3 nm in apparent height at a post annealing temperature of 100 °C, thus suggesting that also for these molecular complexes the horizontal arrangement is preferred (Figure S34e). In this horizontal arrangement, the optical activity of the chromophore is expected to be quenched and indeed no molecular features in the photon spectra were observed. Formation of clusters consisting of molecules in more upright configurations were not observed.

Conclusions

In summary, three tripodal model compounds consisting of a triphenylmethane platform with three acetyl-protected thiol anchors in the *meta* position substituted with different core-substituted NDI chromophores linked via alkyne linker have been synthesised and fully characterised. In a modular approach, the alkyne-decorated rigid tripodal platform was fused with various NDI chromophores by Sonogashira coupling. For this purpose, asymmetric NDI subunits were developed, and their electronic properties were tuned by their core substitu-

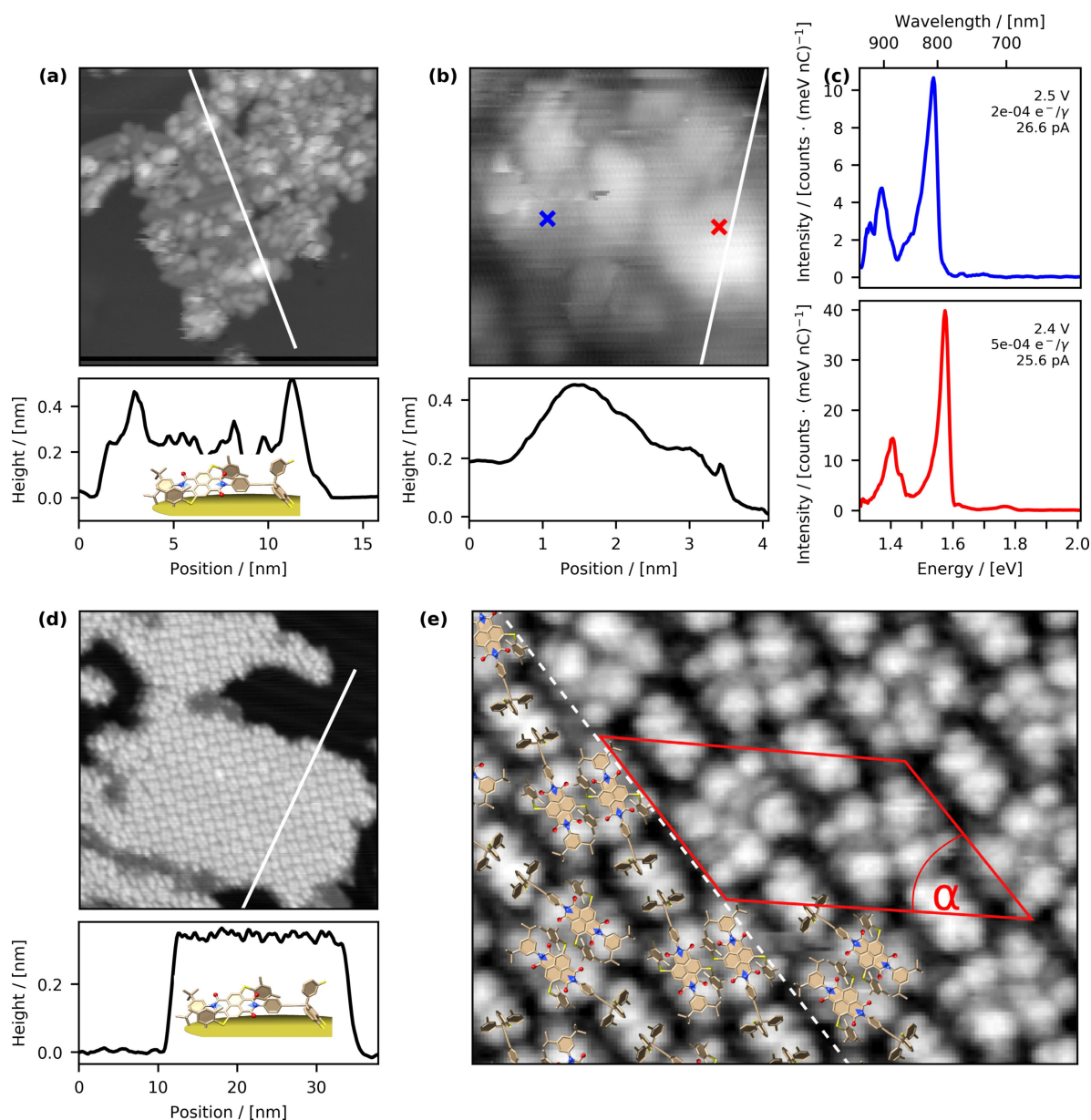


Figure 6. Adsorption and electroluminescence of **Tpd-sNDI**. a) Unordered island structure of **Tpd-sNDI**. The cross section taken along the white line shows a typical height of 0.3 to 0.4 nm. Molecular model not to scale. Sample bias: -1.4 V, tunnelling current: 2 pA, scan width: 15 nm. b) Unordered cluster of **Tpd-sNDI** with a maximal apparent height of 0.4 nm above the surrounding island (see cross section along the white line). Sample bias: 2.4 V, tunnelling current: 5 pA, scan width: 4 nm. c) Typical photon spectra recorded at the positions indicated by the blue and red crosses in (b). Integration times of 4 s were used. Bias voltage, yield and average current during the acquisition as indicated in the graph c). d) Molecular model not to scale. Sample bias: 1.8 V, tunneling current 3 pA. (e) Close up scan of an ordered island with molecular models superimposed to scale. Adjacent rows are mirrored and translated along the dashed white line. The red line indicates a possible unit cell. Sample bias: 2.6 V, tunneling current 8 pA.

ents. Structure-property correlations revealed the influence of the core substituents on optical and electrochemical properties of these model compounds.

Moreover, the self-assembly features of all three tripodal chromophores were analysed after spray deposition on Au (111) surfaces by low-temperature ultra-high-vacuum STM with the electroluminescence setup. These surface studies demonstrated that all tripodal molecules can be deposited in sub-monolayer concentration by “spraying” techniques, and after an annealing procedure, tend to mainly adsorb in a horizontal

configuration as suggested by their arrangement in flat islands. Both **Tpd-hNDI** and **Tpd-sNDI** molecules arrange in a close-packed pairwise fashion and form islands with a long-range lateral order upon annealing at 180°C . At some positions, these molecules formed clusters with an apparent height clearly exceeding that of the surrounding islands. According to the apparent height, these clusters are composed of either multilayers of horizontally aligned molecules, or a monolayer of upright oriented molecules in a less stable configuration. The lateral size clearly suggests that these clusters are composed of

several molecules. In photon spectra, these clusters of molecules showed sharp peaks that are clearly distinct from the plasmonic light of the same tip. Extensive low-temperature UHV-STML studies of these molecules deposited on Au(111) by spray deposition revealed that, at most, a minority of the tripodal chromophores are standing upright and show luminescence; the majority are lying flat on the gold substrate. Even so, only a small minority of the spray-deposited molecules arrange in luminescent clusters, their recorded high electroluminescence yields of up to 6×10^{-3} in the STML experiment not only support the hypothesis of upright standing and decoupled NDI chromophores, but also showcase their potential in highly efficient OLED devices.

Our current work is thus geared towards increasing control over the surface geometry of these chromophores by improving the ordering power of the tripodal architecture.

Experimental Section

Materials: All starting materials and reagents were purchased from commercial suppliers (Alfa Aesar, Sigma-Aldrich, TCI Chemicals Europe (Zwijndrecht, Belgium), Merck and used without further purification. Solvents utilised for crystallisation, chromatography and extraction were used in technical grade. Anhydrous tetrahydrofuran and CD_2Cl_2 were taken from MBraun Solvent Purification System equipped with drying columns. Triethylamine was dried and distilled from CaH_2 under nitrogen. TLC was performed on silica gel 60 F254 plates, spots were detected by fluorescence quenching under UV light at 254 and 366 nm. Column chromatography was performed on silica gel 60 (particle size 0.040–0.063 mm).

Equipment and measurements: All NMR spectra were recorded on a Bruker Avance 500 spectrometer at 25 °C in CDCl_3 , CD_2Cl_2 or MeOD. ^1H NMR (500 MHz) spectra were referred to the solvent residual proton signal (CDCl_3 , $\delta_{\text{H}} = 7.26$ ppm; CD_2Cl_2 , $\delta_{\text{H}} = 5.32$ ppm; MeOD, $\delta_{\text{H}} = 3.31$ ppm). ^{13}C NMR (126 MHz) with total decoupling of protons were referred to the solvent (CDCl_3 , $\delta_{\text{C}} = 77.16$ ppm; CD_2Cl_2 , $\delta_{\text{C}} = 53.84$ ppm; MeOD, $\delta_{\text{C}} = 49.00$ ppm). UV-Vis-NIR absorption spectra were recorded with a Cary 5000 Scan spectrophotometer in a 1 cm quartz cell at ambient temperature (excitation coefficient ϵ [$\text{L mol}^{-1} \text{cm}^{-1}$] is given below). Fluorescence spectra were measured with a Varian Cary Eclipse Fluorescence spectrometer at room temperature in a 1 cm quartz cell. The molecules **sNDI**, **10** and **Tpd-sNDI** were excited at 370 nm and both excitation and emission slits were set to 20 nm. The molecules **nNDI**, **11** and **Tpd-nNDI** were excited at 366 nm and both excitation and emission slits were set to 10 nm. EI MS spectra were recorded with a Thermo Trace 1300-ISQ GC/MS instrument (samples were dissolved in dichloromethane or introduced directly using direct injection probes DIP, DEP) and m/z values are given along with their relative intensities [%] at an ionisation voltage of 70 eV. High-resolution mass spectra were recorded with a Bruker Daltonics (ESI microTOF-QII) mass spectrometer. IR spectra were recorded with a Nicolet iS50 FTIR spectrometer under ATP mode. Analytical samples were dried at 40–100 °C under reduced pressure (10^{-2} mbar). Melting points were measured with a Büchi Melting point M-560 apparatus and are uncorrected. Elemental analyses were obtained with a Vario MicroCube CHNS analyser. The values are expressed in mass percentage. Cyclic voltammetry (CV) experiments were carried out with a Gamry potentiostat, connected to a C3 standard electrochemical cell. Glassy carbon was used as the working electrode, a platinum wire as the counter electrode and Ag/AgNO_3 as the reference electrode. Ferrocene was used as an internal standard and was added after

each series of measurements. The junction potential was corrected to the reference electrode afterwards. The molecules (0.1 mM) were dissolved in 0.1 M solution of Bu_4NPF_6 as an electrolyte in CH_2Cl_2 , and the solution was purged with argon for 10 min before the measurement was taken. Scan rate of the CV measurements was 100 mV s^{-1} and all experiments were performed under ambient conditions at room temperature. All STM measurements were performed in a homebuilt STM at about 4.4 K in UHV (10^{-10} mbar). This STM is equipped with a photon collection system that allows to analyse light that is emitted from the tunnel junction.^[20] All photon spectra were corrected for the energy-dependent detector efficiency (Figure S34a). Electroluminescence count rates are normalised by energy resolution and charge injected (labelled as counts per meV and nC). A clean Au(111) substrate was prepared by argon sputtering at 1.5 kV and subsequent annealing to about 500 °C. Molecules were dissolved in CH_2Cl_2 ($c \sim 1 \text{ mg/mL}$) and an amount of about 1 μL was being sucked into a vacuum chamber ($p \sim 10^{-3}$ mbar) through an aperture of about 0.15 mm. The clean gold surface placed inside the chamber was exposed to the spray formed at the aperture. After deposition, samples were transferred in situ into the ultra-high vacuum (UHV) and were annealed at 100/180 °C in order to promote deprotection of the thiol anchoring groups and to facilitate ordered arrangements of the molecules.^[47] This deposition technique has two major advantages for STM studies: First, the amount of impurities from the solvent is minimised by reducing the amount of solvent deposited onto the sample. Second, deposition of the solution by spraying results in a number of tiny droplets landing randomly across the sample. This leads to an inhomogeneous local coverage, higher in the centre of those former droplets, lower towards the borders. By moving the scan area of our STM, we are able to study different local coverages within one sample (sample size of $9 \times 3 \text{ mm}$). Post annealing leads to a more uniform adsorption configuration on the local scale, but still the coverage is highly variable across the sample. The classical incubation method by immersing gold substrates in thiol solutions for a few hours turned out not to be suitable for our UHV-STM experiments.^[40]

Experimental details and synthetic procedures: The synthesis of 3,3,3-tris(3-methoxyphenyl)propyne **1** was previously reported by Garcia-Garibay et al.^[44] 2,6-Dichloronaphthalene-1,4,5,8-tetracarboxylic acid dianhydride **7** was synthesised in four reaction steps by following a literature procedure.^[9] Detailed synthetic procedures along with complete characterisation data and copies of NMR spectra for all new compounds are given in the Supporting Information.

Acknowledgements

We acknowledge financial support by the Helmholtz Research Program STN (“Science and Technology of Nanosystems”), DFG grant (MA 2605/6-1) and the DAAD grant (57299294). The authors also thank the Institute of Nanotechnology (INT), Karlsruhe Institute of Technology (KIT) for ongoing support. M.M. acknowledges support by the 111 Project (90002-18011002). Open access funding enabled and organized by Projekt DEAL.

Conflict of Interest

The authors declare no conflict of interest.

Keywords: cyclic voltammetry · electroluminescence · naphthalene diimides · scanning probe microscopy · tripodal platforms

- [1] G. Hong, X. Gan, C. Leonhardt, Z. Zhang, J. Seibert, J. M. Busch, S. Bräse, *Adv. Mater.* **2021**, *33*, 2005630.
- [2] U. Mitschke, P. Bäuerle, *J. Mater. Chem.* **2000**, *10*, 1471–1507.
- [3] N. Sakai, J. Mareda, E. Vauthey, S. Matile, *Chem. Commun.* **2010**, *46*, 4225–4237.
- [4] M. Al Kobaisi, S. V. Bhosale, K. Latham, A. M. Raynor, S. V. Bhosale, *Chem. Rev.* **2016**, *116*, 11685–11796.
- [5] J. Hak, S. Sabin-Lucian, W. Y. Lee, M. Könnemann, H. W. Höffken, C. Röger, R. Schmidt, Y. Chung, W. C. Chen, F. Würthner, Z. Bao, *Adv. Funct. Mater.* **2010**, *20*, 2148–2156.
- [6] F. Würthner, M. Stolte, *Chem. Commun.* **2011**, *47*, 5109–5115.
- [7] M. Korzec, S. Kotowicz, K. Łaba, M. Łapkowski, J. G. Malecki, K. Smolarek, S. Maćkowiak, E. Schab-Balcerzak, *Eur. J. Org. Chem.* **2018**, 1756–1760.
- [8] H. F. Higginbotham, P. Pander, R. Rybakiewicz, M. K. Etherington, S. Maniam, M. Zagorska, A. Pron, A. P. Monkman, P. Data, *J. Mater. Chem. C* **2018**, *6*, 8219–8225.
- [9] H. Vollmann, H. Becker, M. Corell, H. Streeck, *Liebigs Ann.* **1937**, *531*, 159.
- [10] F. Würthner, S. Ahmed, C. Thalacker, T. Debaerdemaeker, *Chem. Eur. J.* **2002**, *8*, 4742–4750.
- [11] S. Erten, Y. Posokhov, S. Alp, S. İçli, *Dyes Pigm.* **2005**, *64*, 171–178.
- [12] D. Shukla, S. F. Nelson, D. C. Freeman, M. Rajeswaran, W. G. Ahearn, D. M. Meyer, J. T. Carey, *Chem. Mater.* **2008**, *20*, 7486–7491.
- [13] C. Thalacker, C. Röger, F. Würthner, *J. Org. Chem.* **2006**, *71*, 8098–8105.
- [14] S. L. Suraru, F. Würthner, *Angew. Chem. Int. Ed.* **2014**, *53*, 7428–7448; *Angew. Chem.* **2014**, *126*, 7558–7578.
- [15] R. E. Dawson, A. Hennig, D. P. Weimann, D. Emery, V. Ravikumar, J. Montenegro, T. Takeuchi, S. Gabutti, M. Mayor, J. Mareda, C. A. Schalley, S. Matile, *Nat. Chem.* **2010**, *2*, 533–538.
- [16] S. Guha, F. S. Goodson, L. J. Corson, S. Saha, *J. Am. Chem. Soc.* **2012**, *134*, 13679–13691.
- [17] C. W. Marquardt, S. Grunder, A. Błaszczak, S. Dehm, F. Hennrich, H. V. Löhneysen, M. Mayor, R. Krupke, *Nat. Nanotechnol.* **2010**, *5*, 863–867.
- [18] N. L. Schneider, F. Matino, G. Schull, S. Gabutti, M. Mayor, R. Berndt, *Phys. Rev. B* **2011**, *84*, 153403.
- [19] K. Kuhnke, C. Große, P. Merino, K. Kern, *Chem. Rev.* **2017**, *117*, 5174–5222.
- [20] K. Edelmann, L. Gerhard, M. Winkler, L. Wilmes, V. Rai, M. Schumann, C. Kern, M. Meyer, M. Wegener, W. Wulfhekel, *Rev. Sci. Instrum.* **2018**, *89*, 123107.
- [21] R. Berndt, J. K. Gimzewski, P. Johansson, *Phys. Rev. Lett.* **1991**, *67*, 3796–3799.
- [22] Y. Zhang, Y. Luo, Y. Zhang, Y. J. Yu, Y. M. Kuang, L. Zhang, Q. S. Meng, Y. Luo, J. L. Yang, Z. C. Dong, J. G. Hou, *Nature* **2016**, *531*, 623–627.
- [23] H. Imada, K. Miwa, M. Imai-Imada, S. Kawahara, K. Kimura, Y. Kim, *Phys. Rev. Lett.* **2017**, *119*, 1–6.
- [24] Z. C. Dong, X. L. Zhang, H. Y. Gao, Y. Luo, C. Zhang, L. G. Chen, R. Zhang, X. Tao, Y. Zhang, J. L. Yang, J. G. Hou, *Nat. Photonics* **2010**, *4*, 50–54.
- [25] B. Doppagne, M. C. Chong, H. Bulou, A. Boeglin, F. Scheurer, G. Schull, *Science* **2018**, *361*, 251–255.
- [26] X. H. Qiu, G. V. Nazin, W. Ho, *Science* **2003**, *299*, 542–546.
- [27] R. Berndt, R. Gaisch, J. K. Gimzewski, B. Reihl, R. R. Schlittler, W. D. Schneider, M. Tschudy, *Science* **1993**, *262*, 1425–1427.
- [28] Y. M. Kuang, Y. J. Yu, Y. Luo, J. Z. Zhu, Y. Liao, Y. Zhang, Z. C. Dong, *Chin. J. Chem. Phys.* **2016**, *29*, 157–160.
- [29] J. Repp, G. Meyer, S. M. Stojković, A. Gourdon, C. Joachim, *Phys. Rev. Lett.* **2005**, *94*, 1–4.
- [30] Z. C. Dong, X. L. Guo, A. S. Trifonov, P. S. Dorozhkin, K. Miki, K. Kimura, S. Yokoyama, S. Mashiko, *Phys. Rev. Lett.* **2004**, *92*, 1–4.
- [31] M. Valášek, M. Mayor, *Chem. Eur. J.* **2017**, *23*, 13538–13548.
- [32] M. Valášek, M. Lindner, M. Mayor, *Beilstein J. Nanotechnol.* **2016**, *7*, 374–405.
- [33] T. Ijaz, B. Yang, R. Wang, J. Zhu, A. Farrukh, G. Chen, G. Franc, Y. Zhang, A. Gourdon, Z. Dong, *Appl. Phys. Lett.* **2019**, *115*, 1–5.
- [34] S. E. Zhu, Y. M. Kuang, F. Geng, J. Z. Zhu, C. Z. Wang, Y. J. Yu, Y. Luo, Y. Xiao, K. Q. Liu, Q. S. Meng, L. Zhang, S. Jiang, Y. Zhang, G. W. Wang, Z. C. Dong, J. G. Hou, *J. Am. Chem. Soc.* **2013**, *135*, 15794–15800.
- [35] F. Matino, G. Schull, F. Köhler, S. Gabutti, M. Mayor, R. Berndt, *Proc. Natl. Acad. Sci. USA* **2011**, *108*, 961–964.
- [36] F. L. Otte, S. Lemke, C. Schütt, N. R. Krekieleh, U. Jung, O. M. Magnussen, R. Herges, *J. Am. Chem. Soc.* **2014**, *136*, 11248–11251.
- [37] V. Rai, L. Gerhard, Q. Sun, C. Holzer, T. Repän, M. Krstić, L. Yang, M. Wegener, C. Rockstuhl, W. Wulfhekel, *Nano Lett.* **2020**, *20*, 7600–7605.
- [38] M. Lindner, M. Valášek, M. Mayor, T. Frauhammer, W. Wulfhekel, L. Gerhard, *Angew. Chem. Int. Ed.* **2017**, *56*, 8290–8294; *Angew. Chem.* **2017**, *129*, 8405–8410.
- [39] T. Frauhammer, L. Gerhard, K. Edelmann, M. Lindner, M. Valášek, M. Mayor, W. Wulfhekel, *Phys. Chem. Chem. Phys.* **2021**, *23*, 4874–4881.
- [40] M. Lindner, M. Valášek, J. Homberg, K. Edelmann, L. Gerhard, W. Wulfhekel, O. Fuhr, T. Wächter, M. Zharnikov, V. Kolivoška, L. Pospíšil, G. Mészáros, M. Hromadová, M. Mayor, *Chem. Eur. J.* **2016**, *22*, 13218–13235.
- [41] J. Homberg, M. Lindner, L. Gerhard, K. Edelmann, T. Frauhammer, Y. Nahas, M. Valášek, M. Mayor, W. Wulfhekel, *Nanoscale* **2019**, *11*, 9015–9022.
- [42] H. Valkenier, E. H. Huisman, P. A. Van Hal, D. M. De Leeuw, R. C. Chiechi, J. C. Hummelen, *J. Am. Chem. Soc.* **2011**, *133*, 4930–4939.
- [43] T. Sakata, S. Maruyama, A. Ueda, H. Otsuka, Y. Miyahara, *Langmuir* **2007**, *23*, 2269–2272.
- [44] J. E. Nuñez, T. A. V. Khuong, L. M. Campos, N. Farfán, H. Dang, S. D. Karlen, M. A. Garcia-Garibay, *Cryst. Growth Des.* **2006**, *6*, 866–873.
- [45] J. E. Nuñez, A. Natarajan, S. I. Khan, M. A. Garcia-Garibay, *Org. Lett.* **2007**, *9*, 3559–3561.
- [46] G. I. Feutrill, R. N. Mirrington, *Tetrahedron Lett.* **1970**, 1327–1328.
- [47] M. Valášek, K. Edelmann, L. Gerhard, O. Fuhr, M. Lukas, M. Mayor, *J. Org. Chem.* **2014**, *79*, 7342–7357.
- [48] A. Błaszczak, M. Fischer, C. Von Hänisch, M. Mayor, *Helv. Chim. Acta* **2006**, *89*, 1986–2005.
- [49] R. Fernando, Z. Mao, E. Muller, F. Ruan, G. Sauvé, *J. Phys. Chem. C* **2014**, *118*, 3433–3442.
- [50] S. Chopin, F. Chaignon, E. Blart, F. Odobel, *J. Mater. Chem.* **2007**, *17*, 4139–4146.
- [51] J. Pommerehne, H. Vestweber, W. Guss, R. F. Mahrt, H. Bässler, M. Porsch, J. Daub, *Adv. Mater.* **1995**, *7*, 551–554.
- [52] R. S. K. Kishore, O. Kel, N. Banerji, D. Emery, G. Bollot, J. Mareda, A. Gomez-Casado, P. Jonkheijm, J. Huskens, P. Maroni, M. Borkovec, E. Vauthey, N. Sakai, S. Matile, *J. Am. Chem. Soc.* **2009**, *131*, 11106–11116.
- [53] J. L. Bredas, R. Silbey, D. S. Boudreaux, R. R. Chance, *J. Am. Chem. Soc.* **1983**, *105*, 6555–6559.
- [54] C. Q. Ma, M. Fonrodona, M. C. Schikora, M. M. Wienk, R. A. J. Janssen, P. Bäuerle, *Adv. Funct. Mater.* **2008**, *18*, 3323–3331.
- [55] R. Fernando, F. Etheridge, E. Muller, G. Sauvé, *New J. Chem.* **2015**, *39*, 2506–2514.
- [56] Y. Zhao, G. Huang, C. Besnard, J. Mareda, N. Sakai, S. Matile, *Chem. Eur. J.* **2015**, *21*, 6202–6207.
- [57] C. Röger, F. Würthner, *J. Org. Chem.* **2007**, *72*, 8070–8075.
- [58] X. Tao, Z. C. Dong, J. L. Yang, Y. Luo, J. G. Hou, J. Aizpuru, *J. Chem. Phys.* **2009**, *130*, 084706.
- [59] J. Aizpuru, S. P. Apell, R. Berndt, *Phys. Rev. B* **2000**, *62*, 2065–2073.
- [60] B. Doppagne, M. C. Chong, E. Lorchat, S. Berciaud, M. Romeo, H. Bulou, A. Boeglin, F. Scheurer, G. Schull, *Phys. Rev. Lett.* **2017**, *118*, 127401.
- [61] G. Chen, Y. Luo, H. Gao, J. Jiang, Y. Yu, L. Zhang, Y. Zhang, X. Li, Z. Zhang, Z. Dong, *Phys. Rev. Lett.* **2019**, *122*, 177401.
- [62] L. Zhang, Y. J. Yu, L. G. Chen, Y. Luo, B. Yang, F. F. Kong, G. Chen, Y. Zhang, Q. Zhang, Y. Luo, J. L. Yang, Z. C. Dong, J. G. Hou, *Nat. Commun.* **2017**, *8*, 1–7.
- [63] G. Reecht, F. Scheurer, V. Speisser, Y. J. Dappe, F. Mathevet, G. Schull, *Phys. Rev. Lett.* **2014**, *112*, 047403.

Manuscript received: April 8, 2021

Accepted manuscript online: June 21, 2021

Version of record online: July 22, 2021